Soft Matter

Accepted Manuscript

Journal Name

ARTICLE TYPE

Hard sphere packings within cylinders

Lin Fu,[a] William Steinhardt,[b] Hao Zhao,[a] Joshua E. S. Socolar,[b] and Patrick Charbonneau[*ab]

Arrangements of identical hard spheres confined to a cylinder with hard walls have been used to model experimental systems, such as fullerenes in nanotubes and colloidal wire assembly. Finding the densest configurations, called close packings, of hard spheres of diameter σ in a cylinder of diameter D is a purely geometric problem that grows increasingly complex as D/σ increases, and little is thus known about the regime for $D > 2.873\sigma$. In this work, we extend the identification of close packings up to $D = 4.00\sigma$ by adapting Torquato-Jiao's adaptive-shrinking-cell formulation and sequential-linear-programming (SLP) technique. We identify 17 new structures, almost all of them chiral. Beyond $D \approx 2.85\sigma$, most of the structures consist of an outer shell and an inner core that compete for being close packed. In some cases, the shell adopts its own maximum density configuration, and the stacking of core spheres within it is quasiperiodic. In other cases, an interplay between the two components is observed, which may result in simple periodic structures. In yet other cases, the very distinction between core and shell vanishes, resulting in more exotic packing geometries, including some that are three-dimensional extensions of structures obtained from packing hard disks in a circle.

1 Introduction

Packing problems, i.e., identifying optimal configurations of a set of hard geometric objects in space without overlap, are NP-hard optimization problems[1]. Of these problems, packings of hard spheres (HS) have been the most extensively investigated because of their dual physical generality and mathematical elegance. For instance, in condensed matter hard sphere packings help explain both the ordering of binary alloys[2–4] and the persistence of disorder in metallic glass formers[5]. For a given set of constraints, the densest packing, referred to as the close packed arrangement, is of particular interest. Mathematical demonstrations of the optimality of these packings present prestigious challenges to surmount. In two dimensions, the triangular lattice of disks in which each touches six others has long been known to be the close packed arrangement[6], but the proof of the Kepler conjecture for hard spheres in three dimensions was only recently obtained[7] (with much fanfare[6]), and in higher dimensions demonstrations are an absolute scarcity[8,9].

Although packing hard objects in infinite spaces can be a reasonable model for describing the structure of bulk materials, in confined systems boundaries can play a substantial role. Identifying close packings in bounded spaces is also motivated by

the wide variety of situations in which objects are stored in containers of different shapes[10–12]. Many variants of this problem have thus been considered by mathematicians and physicists, including disks in a circle[13–15], a rectangle or a strip[16,17] in two dimensions, and spheres in a sphere, a cube[18,19] or a parallelepiped[20] in three dimensions. Irrespective of the dimensionality of the packed objects, however, the above packing problems are all quasi-zero-dimensional, because extrapolating to the small system limit gives a simple point. Packing objects between planes, i.e., in quasi-two-dimensional confinement, has also been intensely studied[21–23], notably in order to understand the transition from two-step to first-order melting as the thickness is increased from a monolayer to a bulk system.

The intermediate case of quasi-one-dimensional confinement models a number of experiments, including the trapping of fullerenes in nanotubes[24,25], the formation of colloidal wires[26] and the self-assembly of nanoparticles in cylindrical domains[27–29], yet has received substantially less attention than other confinement geometries. Existing studies nonetheless suggest that these systems can display a variety of remarkable structural features. Early experimental work, for instance, suggested that a broad range of structures could be obtained[30], including elaborate spiral structures. The first efforts by Pickett et al. to systematically identify close packings of HS of diameter σ in cylinders of diameters D detailed the emergence of spontaneous helical chirality[31]; and Mughal et al.'s extension of this work from

[a] Duke University, Department of Chemistry, Durham, NC 27708, USA. E-mail: patrick.charbonneau@duke.edu
[b] Duke University, Department of Physics, Durham, NC 27708, USA.

$D = 2.155\sigma$ to $D = 2.873\sigma$ showed how line slips allow helical structures to continuously transform into one another[32].

Because the largest cylinders studied remain quite far from the bulk limit, a rich set of structural features is to be expected in wider cylinders as well. Many of the existing tools for finding dense packings are, however, insufficient in this regime. Earlier analyses relied on simulated annealing[31,32], whose computational efficiency is too limited for finding packings with a separate inner core and outer shell. Algorithms based on sequential deposition are much more expedient[33], but the final structure they generate depends too sensitively on the choice of underlying template for them to be of broad applicability. Although a genetic algorithm scheme (akin to that used in Ref.[3]) can search configuration space more broadly, the growing structural complexity of the packings with D necessitates unit cells that are too large for the approach to remain computationally tractable.

In this work, we improve the computational efficiency for finding close packings of monodisperse HS in cylinders with $D > 2.873\sigma$ by instead using an adaptive-shrinking cell and a sequential-linear-programming (SLP) technique[34]. This approach confirms earlier results for $D \leq 2.86\sigma$ and extends our knowledge of close packed structures up to $D = 4.00\sigma$. Interestingly, many of the new structures appear to be quasiperiodic and some even present fairly exotic geometries. In Section 2, we describe the SLP computational method, in Section 3 we present the SLP results for different ranges of cylinder diameters, and in Section 4 we specifically analyze the quasiperiodic structures observed in the range $2.988\sigma \leq D \leq 3.42\sigma$ using a sinking algorithm developed for this problem.

2 Sequential Linear Programming Method

In order to identify close packings of HS in cylinders, we adapt the SLP method of Torquato and Jiao[34] to this geometry. For convenience, we describe configurations using cylindrical coordinates with z, r, and θ representing the axial, radial and angular components, respectively. For our search procedure, we consider a fixed number of spheres in a finite cylinder with periodic boundary conditions that match the top of the cylinder to the bottom with a twist. In other words, the entire volume of the cylinder is taken as a unit cell with a one-dimensional periodicity. The infinite structure consists of spheres centered at

$$\mathbf{r}_{ij} = \mathbf{r}_i + n_j \boldsymbol{\lambda} , \tag{1}$$

where $\mathbf{r}_i$ ($i = 1, 2, ...$) are the particle positions within a unit cell, $n_j \in \mathbb{Z}$, and $\boldsymbol{\lambda} = (\lambda_r, \lambda_\theta, \lambda_z)$ is the lattice vector. For our system, λ_z is the height of the unit cell, λ_θ is the twist angle, and $\lambda_r = 0$. Note that for helical structures, the twist angle is necessary because $\Delta\theta$ between two successive particles in a helix may not be a rational fraction of 2π. The volume of a unit cell is thus

$$v_u = \pi (D/2)^2 \lambda_z , \tag{2}$$

and the lattice packing fraction can be expressed as

$$\eta = \frac{N v_s}{v_u} , \tag{3}$$

where N is the number of particles in a unit cell and v_s is the volume of a sphere of diameter σ.

A each optimization step, we allow the N particles in the unit cell to move as well as changes to the unit cell height, λ_z, and twist angle, λ_θ. Denoting particle displacements $\Delta\mathbf{r}$, the matrix specifying changes to the unit cell $\boldsymbol{\varepsilon}$, the new particle positions $\mathbf{r}^n$, and the new lattice vector $\boldsymbol{\lambda}^n$, we have

$$\boldsymbol{\lambda}^n = (\mathbf{I} + \boldsymbol{\varepsilon})\boldsymbol{\lambda} \tag{4}$$

$$\boldsymbol{\varepsilon} = \begin{bmatrix} 0 & 0 & 0 \\ 0 & \varepsilon_\theta & 0 \\ 0 & 0 & \varepsilon_z \end{bmatrix} \tag{5}$$

$$\mathbf{r}^n = (r_r + \Delta r_r, r_\theta + \Delta r_\theta, (1 + \varepsilon_z)(r_z + \Delta r_z)) . \tag{6}$$

Note that the twist angle is not continuously shearing the particles within the unit cell, but is only a property of the boundary conditions. It thus only appears in $\mathbf{r}^n$ for boundary particles.

In order to find the maximum packing density we must solve the following problem:

$$\text{minimize } v_u$$

subject to

$$r_{ij}^n \geq \sigma , \ \forall \ ij \text{ neighbor pairs}, \tag{7}$$

$$r_{ir} + \Delta r_{ir} + \sigma/2 \leq D/2, \ \forall \ i = (1, 2, ..., N). \tag{8}$$

The first condition corresponds to the hard-sphere constraint and the second to the hard-wall constraint. Because during the optimization D is fixed, minimizing v_u is equivalent to minimizing λ_z. The packing problem then becomes a standard constrained optimization problem, and the constraints can be linearized (by Taylor expansion), allowing the use of linear-programming solvers[34,35]. The optimization problem at each step then becomes

$$\text{minimize} : \varepsilon_z,$$

subject to

$$r_{ij}^n \geq \sigma, \forall \ ij \text{ neighbor pairs} \tag{9}$$

$$r_{ir} + \Delta r_r + \sigma_i/2 \leq D/2, \ \forall \ i \tag{10}$$

$$|\Delta r_{ir}| \leq \Delta r_r^{upper}, \ \forall \ i \tag{11}$$

$$|\Delta r_{i\theta}| \leq \Delta r_\theta^{upper}, \ \forall \ i \tag{12}$$

$$|\Delta r_{iz}| \leq \Delta r_z^{upper}, \ \forall \ i \tag{13}$$

$$|\varepsilon_\theta| \leq \varepsilon_\theta^{upper} \tag{14}$$

$$|\varepsilon_z| \leq \varepsilon_z^{upper}, \tag{15}$$

with algorithmic bounds that are sufficiently small so as to limit large particle overlaps, which are a consequence of linearization and are eliminated by counter-productively expanding the unit cell, but not so small so as to slow down convergence. Here,

optimal bounds on particle displacements and volume changes are found to be roughly $\Delta r_{\mathrm{r}}^{\mathrm{upper}} = \Delta r_{\mathrm{z}}^{\mathrm{upper}} = \varepsilon_{\mathrm{z}}^{\mathrm{upper}} = 0.001\sigma$, and $\Delta r_{\theta}^{\mathrm{upper}} = \varepsilon_{\theta}^{\mathrm{upper}} = 0.001$ radians. The overall packing optimization can thus be done sequentially, meaning that the optimal solution for a given step is used as input for the subsequent one, until convergence is achieved. Operationally, we accept a solution as having converged when the difference between two iterations $|\Delta v_{\mathrm{u}}| < v_{\mathrm{tol}}$, where $v_{\mathrm{tol}} = 10^{-6}$. Note that because this criterion is independent of the unit cell size, the final unit cell volume is determined less precisely for smaller system sizes , but this effect is negligible on the scale of the figures and of the other numerical results reported here.

Recall that for periodic structures, close packing can only be obtained when $N = n_{\mathrm{c}} N_{\mathrm{c}}$, where n_{c} is a positive integer and N_{c} is the number of particles in the unit cell. For regimes where the densest structure is known (and periodic), i.e., at small diameters, we choose $n_{\mathrm{c}} \geq 3$. For the rest of the diameter range, however, no systematic studies have previously been undertaken, and only a few structures have been proposed[30,36]. Where N_{c} is not a priori known, we resort to scanning system sizes with $N = 48$ to $N = 150$. If the close packing is actually periodic with $N_c \leq 150$, it is identified properly, and the N that yields the highest density is an integer multiple of N_{c}. One can then check factors of this N to identify N_{c}. For systems where the close packed arrangement is not periodic or where $N_c > 150$, the algorithm finds the best periodic approximant within this regime of N.

3 SLP Results
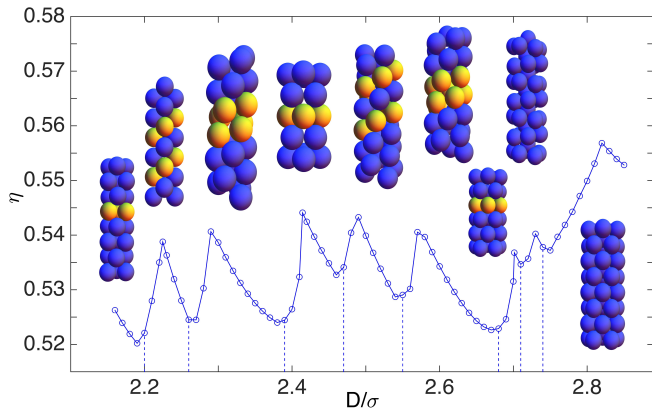
Fig. 1 Close packing densities for $2.16\sigma \leq D \leq 2.86\sigma$. Configurations are depicted at density maxima. Yellow particles are part of a same helix. In this regime, the results are in complete agreement with those of Ref. [37]. Figure 2 presents results for $D \geq 2.86\sigma$.

Using the SLP method, we identified candidate structures for HS close packing from $D = 2.16\sigma$ to $D = 4.00\sigma$. For $D \leq 2.862$, we reproduce previously reported results[32] (Fig. 1), but we obtain denser structures than Mughal et al. for $2.862\sigma < D < 2.873\sigma$ (Fig. 2 inset). This discrepancy is likely due to the difference in system sizes between the two studies. The structures obtained for this regime in Ref.[32] had unit cells with either $N = 7$ or 15 particles, while our system size varies from $N = 24$ to 150, and the densest structures are found to have $50 \leq N \leq 85$. The origin of

this strong system size dependence likely lies in the complex periodicity, i.e., the large N_c, of the packings in this regime, or to their potential aperiodicity. (We come back to this point in Section 4.)

SLP identifies 17 distinct structures and their deformations over $2.873\sigma \leq D \leq 4.00\sigma$ (Fig. 2). The structures depicted in Figure 2 are local maxima in $\eta(D)$. Most of the structures in this regime have two well-defined layers: an outer shell and an inner core. In structures for which this definition makes geometrical sense, the outer shell is comprised of particles that are touching the wall, or nearly so, and which form a corrugated cylinder of diameter roughly $D - \sigma$ that contains the particles comprising the inner core. Because many of the outer shells are themselves close packings of spheres disks on the inner surface of the cylinder, they can be described using the phyllotactic notation for helices, (l,m,n), with $l = m + n$ and $m > n$, where l, m and n are the number of helices, using the three possible helix definitions (Fig. 3)[37]. The parameters defining some of these helical outer shells are listed in Table 1. For simplicity, we denote below structures with the helix whose height difference, Δz, between two successive particles within that helix is minimal, and $\Delta \theta$ is thus the angular coordinate difference between two successive particles within that helix (Fig. 3a). Based on these definitions, we note that $\lambda_z = (N_s/l)\Delta z$ and $\lambda_\theta = \mod_{2\pi}((N_s/l)\Delta \theta)$, where N_s is the number of shell particles in the unit cell.

Intermediate structures can be obtained by continuously transforming local density maxima. Some are uniform radial expansions (or compressions) of these structures, accompanied with a compression (or expansion) in z, while other structures undergo a line-slip, which is a slip between two helices, keeping the relative position of the other helices constant[32]. Because a helix can be defined in three different ways (Fig. 3), each maximal density structure presents up to six corresponding line-slip possibilities (two directions for each type of slip), although symmetry can reduce this number.

In the following subsections we present an overview of different D regimes over which the packings we obtain share a number of structural features.

3.1 Structures for $D < 2.86\sigma$

In this regime, all the structures are periodic and have a simple mathematical description. Most of them are simple helices. The last two structures, however, are non-helical and contain an inner core (Fig. 1). HS close packing for $2.71486\sigma \leq D \leq 2.74804\sigma$ has D_5 symmetry with a close packed inner core, and can be constructed as a packing of spindles of nearly regular tetrahedra. The optimal structure for $2.74804\sigma \leq D \leq 2.8481\sigma$ has instead a unit cell of 11 particles – an inner particle sandwiched between two staggered five-particle rings – that is reminiscent of a stacking of ferrocene molecules. Note, however, that neither the inner core nor the outer shell of this last structure are separately close packed.

3.2 Structures for $2.86\sigma \leq D < 2.988\sigma$

For $D \geq 2.86\sigma$, packings do not have simple analytical descriptions. The competition between the inner core and the outer
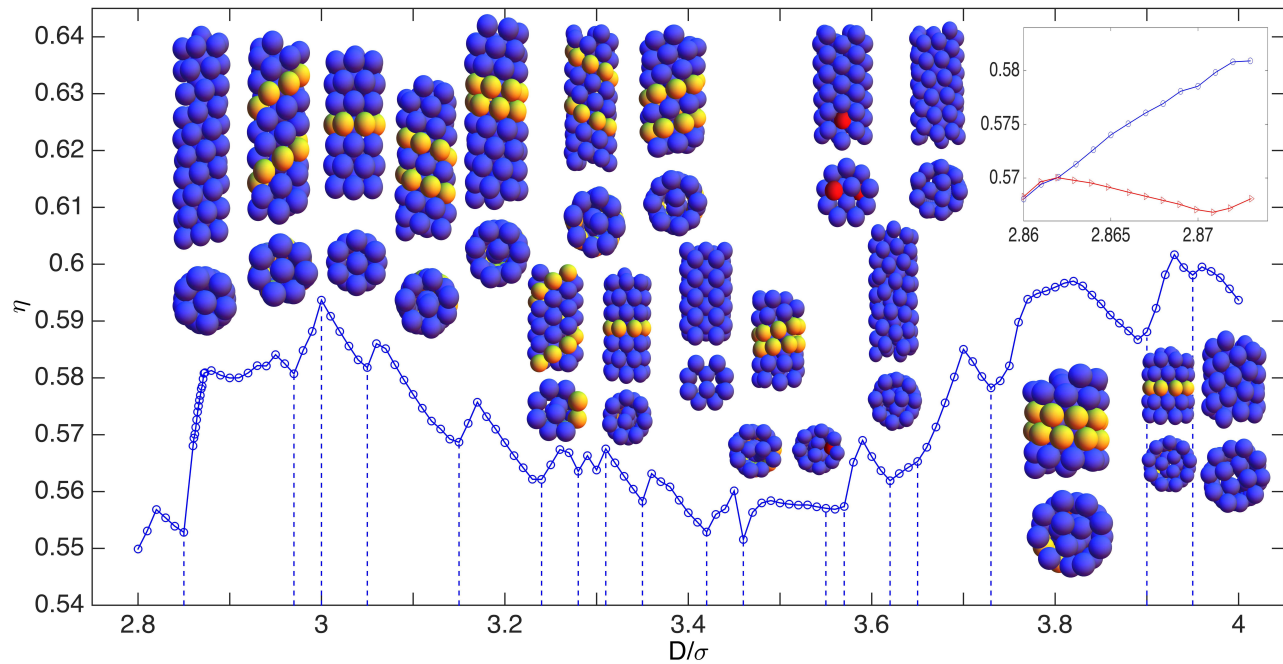
Fig. 2 Close packing densities for $D = 2.85 - 4.00\sigma$. Configurations are depicted at the density maxima. Yellow particles are part of a same helix or its line-slip structure, as described by the phyllotactic notation, and red particles are hoppers (see text for details). Note that some configurations do not have a well-defined helical structure. The inset shows the difference between Mughal et al.'s (red triangles) and the current (blue circles) results for $2.86\sigma < D < 2.875\sigma$.

Table 1 Structural parameters and properties of close packed outer shells for different cylinder diameters. Quantities are rounded to the last digit

Notation	D/σ	$\Delta\theta$	$\Delta z/\sigma$	Chirality	Number of helices
(6,5,1)	2.8652	1.1167	0.1538	chiral	1
(6,6,0)	3.0000	1.0472	0.0000	achiral	/
(7,4,3)	3.0038	0.9365	0.4268	chiral	3
(7,5,2)	3.0623	0.9697	0.2759	chiral	2
(7,6,1)	3.1664	0.9507	0.1309	chiral	1
(8,4,4)	3.2630	0.7854	0.5000	achiral	4
(8,5,3)	3.2888	0.8357	0.3706	chiral	3
(7,7,0)	3.3048	0.8976	0.0000	achiral	/
(8,6,2)	3.3615	0.8475	0.2391	chiral	2
(8,7,1)	3.4720	0.8272	0.1139	chiral	1
(9,5,4)	3.5377	0.7220	0.4434	chiral	4
(9,6,3)	3.5818	0.7496	0.3267	chiral	3
(8,8,0)	3.6131	0.7854	0.0000	achiral	/
(9,7,2)	3.6648	0.7512	0.2109	chiral	2
(9,8,1)	3.7805	0.7318	0.1008	chiral	1
(10,5,5)	3.8025	0.6283	0.5000	achiral	5
(10,6,4)	3.8223	0.6624	0.3971	chiral	4
(10,7,3)	3.8800	0.6771	0.2917	chiral	3
(9,9,0)	3.9238	0.6981	0.0000	achiral	/
(10,8,2)	3.9711	0.6738	0.1883	chiral	2
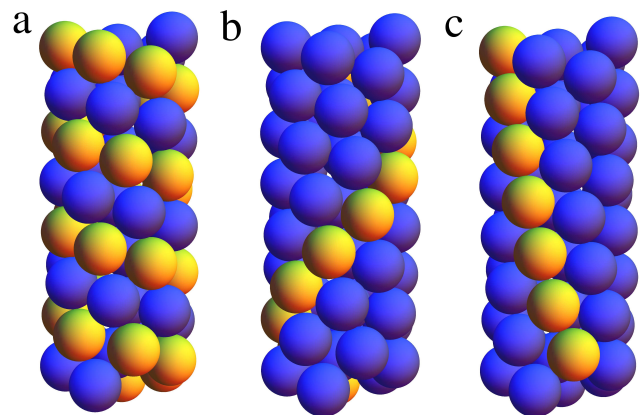
Fig. 3 There exists three different ways to define a helix, and thus six possible line-slip structures. Yellow particles are part of a same helix. This configuration is an example of a $(l,m,n) = (7,5,2)$ helix, where $l = 7$ can be obtained by counting the particle number of the top layer (c), m is depicted in (b), and n in (a). In the text, we select the convention depicted in (a) to denote helices.

shell becomes more complex, because the two layers have different packing requirements, and neither of them systematically wins. For $2.86\sigma \leq D \leq 2.988\sigma$, the inner core dominates. To see why, note that a core particle can only fit into a shell formed by a horizontal layer of 6 spheres when $D \geq 3\sigma$. For $D < 3\sigma$, a core sphere can only fit if these 6 spheres form a helix around it. Every core particle must thus be at the center of a six-particle helix,

which limits its freedom to move within the inner core. For instance, for a perfect (6,5,1) outer shell, for which $D = 2.8652\sigma$, the spacing between two turns of the six-particle helix that forms the outer shell is $6\Delta z = 0.9228\sigma < \sigma$. If the outer shell were itself close packed, then three six-particle helices would only accommodate a single inner particle, leaving large gaps between inner particles. A denser structure is instead obtained by deforming the

outer shell in order to accommodate a denser inner core.

As D approaches 3σ, core particles become increasingly free to move. For $2.97\sigma < D < 3.00\sigma$, the close packed outer shell is a line-slip structure of (7,4,3). The perfect (7,4,3) outer shell at $D = 3.0038\sigma$ has an inner core spacing of $\frac{7}{3}\Delta z = 0.9959(1)\sigma$, which is barely smaller than a particle diameter. Hence, for $2.97\sigma < D < 2.988\sigma$, although the overall structure remains dominated by the inner core, the outer shell barely differs from a close packed, line-slip structure of (7,4,3).

### 3.3 Structures for $2.988\sigma \leq D \leq 3.42\sigma$

For $2.988\sigma \leq D$, the inner core is sufficiently large to allow core particles to move freely within an outer shell, thus greatly reducing their constraint on the outer shell. Note that the lower end of this range is smaller than 3σ because the close packed shell for $2.988\sigma \leq D < 3.000\sigma$ is a line-slip structure of (7,4,3), for which no six outer particles are ever in the same plane. They can thus wrap an inner core without difficulty. Close packed structures from that point on and up to $D = 3.42\sigma$ are found to almost always form a close packed outer shell, independently of the inner core. The local density maxima in Figure 2 for this regime indeed all correspond to the diameters of close packed outer shells (Table 1).

Out of the sequence, the structure with a (8,4,4) outer shell is particularly noteworthy. As for all outer shells with $m = n = \frac{1}{2}l$, this helical structure is achiral – two of the three possible helical directions are equivalent, and $\Delta z = \sigma/2$. As a result, the outer shell consists of straight columns when viewed from the top of the cylinder. The top view of (8,4,4) outer shell and its core is thus very similar to the close packing of hard disks in a circle (Fig. 4a). Two other structures are found to have this property (Fig. 4b and c), but the structure with the (8,4,4) outer shell is the only one that is close packed. Note that a similar phenomenon would likely be observed for a structure with a (10,5,5) outer shell were it to be close packed (which it is not).

The case $D = 3.00\sigma$ is also remarkable. The outer shell is then a close packed structure with staggered six-particle rings, i.e., (6,6,0). The spacing between two rings is $\Delta_\perp = \sigma\sqrt{\sqrt{3}-1} \doteq 0.8556\sigma$. Although core particles placed between the planes of the rings can shift off the cylinder axis, they cannot shift enough to allow a periodic packing of the core with no gaps between successive core spheres. This phenomenon illustrates the difficulty of searching for close packed structures in this regime. Close packed structures may indeed be quasiperiodic and thus not correspond to any finite λ_z or N_c. In the present context, a quasiperiodic structure consists of a periodic shell and a column of core particles with an average vertical separation that is irrational with respect to the height of the unit cell of the shell. Our numerical approach then at best provides a periodic approximant of that structure. In order to consider this issue more carefully, we present an alternate algorithm for studying this regime in Section 4.

3.4 Structures for $D > 3.42\sigma$

For $D > 3.42\sigma$, many of the close packed outer shells are not observed. Instead of remaining disordered or quasiperiodic, the
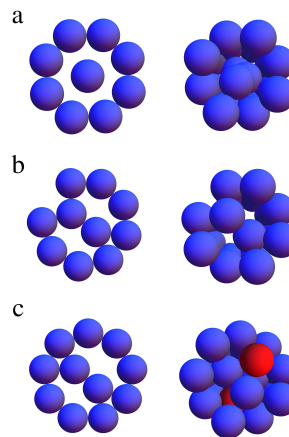
Fig. 4 Comparison between disks in a circle and the top view of spheres in a cylinder at (a) $D = 3.613\sigma$ [38] (circle) and $D = 3.25\sigma$ (cylinder), (b) $D = 3.813\sigma$ [38] (circle) and 3.43σ (cylinder), and (c) $D = 3.924\sigma$ [39] (circle) and 3.58σ (cylinder). Red particles are hoppers. The cylinder outer shells consist of straight columns and only the top layer of particles is visible, so the resulting packings look similar to those of disks in a circle. Note that because the height of neighboring columns is shifted by 0.5σ, the cylinder diameter is smaller than that of the circle and projecting particles onto the cylinder base reveals overlaps.

inner core then forms nearly ordered structure, which imposes many defects on the outer shell. For some of the packings, the defects are so large that they enable the two shells to interpenetrate. The structures in this regime are thus not clearly dominated by any one of the two layers, hence neither of the two shells is typically close packed. For instance, of l-particle staggered ring structures, $(l, l, 0)$, only $l = 6$, 7 and 9 are observed. For $l = 6$ and 7, the inner core is so small that only a lightly zig-zagging chain of particles fits within it; for $l = 9$, the inner core is large enough that a staggered three-particle ring structure fits. For $l = 8$, however, the zig-zagging structure is not very dense, and a two-particle flat pair does not fit. The packing structure thus ends up having a completely different organization: a dense triple helix inner core and an tortuous outer helical shell of eight particles.

The competition between the two shells does not only result in defective compromises, but also yields two novel types of structures. First, some structures are analogous to three-dimensional extensions of packing of hard disks in a circle (Fig. 4b and c). Although the roughly straight columns formed by these structures gives their top view a two-dimensional feel, they are not simple stacks of these packings. As can be seen in Figure 4, projections of particles onto the cylinder base reveals overlaps. The outer shell is an (imperfect) triangular lattice rather than a square lattice, and the outer rings are not flat but form zig-zags. As a result the same three-dimensional version fits in a cylinder with a smaller diameter than the corresponding two-dimensional circle. Second, some structures cannot be neatly divided into shells. For instance, for $3.55\sigma \leq D \leq 3.61\sigma$, although both layers are dense the gap between them is sufficiently large to allow outer particles to hop back and forth between the two shells, keeping η unchanged (Fig. 4c and Fig. 2).

Table 1 indicates that four ten-fold ($l = 10$) outer shells could

potentially be observed for $D \leq 4.00\sigma$. Yet only one appears in the phase sequence, as the last structure. The other three structures are missing, because for $3.62\sigma \leq D \leq 3.94\sigma$ the inner core is just large enough to accommodate a triple helix, and thus a nine-fold helical outer shell better accommodates this inner shell than a ten-fold one.

As discussed in Sec. 3, for $3.00\sigma \leq D \leq 3.42\sigma$, the incommensurability of the two shells may result in structures that are not periodic. Close packed structures thus cannot be obtained using a finite periodic unit cell, which makes the numerical search for packings by SLP extremely challenging (if not impossible) for some regions, e.g. $3.00\sigma \leq D \leq 3.05\sigma$. By contrast, for $D > 3.42\sigma$ the strong interaction between the two shells forces the two to share a same periodicity in some ranges of D (see Supplementary Table S1). There therefore exist in those regions dense periodic structures that can be identified with relative computational ease. The vastness of the configurational space to sample at this point, however, reduces the confidence with which truly close packed structures are then identified.

## 4   Sinking algorithm for $2.988\sigma \leq D \leq 3.42\sigma$

SLP results suggest that for $2.988\sigma \leq D \leq 3.42\sigma$ packings may be quasiperiodic. Despite their relatively simple geometrical description, the true densest structures are then beyond the reach of our numerical algorithm because SLP relies on periodic boundary conditions. Systematically extrapolating the SLP results to infinite system size could sidestep this difficulty, but the range of computationally accessible system sizes is here insufficient for such extrapolation to be of much numerical significance. We thus consider a more directed approach to analyze the infinite-system size limit of these packings. This approach, however, rests on assumptions about the overall structure of packings that are not rigorously justified, and is found to be suboptimal in a few instances.

We first assume that packings in this regime have an outer shell that is close packed along the cylinder wall (see Fig. 5). For $D = 3\sigma$, for instance, the densest outer shell is the (6,6,0) structure. Note, however, that even this seemingly straightforward case would be mathematically nontrivial to demonstrate. The structure cannot be argued to be the densest possible based on the local packing density, because a closed hexagon (or triangle) of spheres on the cylinder surface minimizes the covered area when one diameter of the hexagon is vertical rather than horizontal as in the (6,6,0) structure (Fig. 6). Rigorously proving that (6,6,0) shell is close packed for $D = 3\sigma$ thus remains an open problem. We nonetheless persist in this direction and next assume that each successive core particle falls to its lowest possible position without perturbing the outer shell. These assumptions are broadly consistent with the SLP results, and should allow for slightly denser structures to be obtained by sidestepping the periodicity and finite-size constraints of that algorithm.

For convenience, in the following we define the shell density, ρ_s, as the number of shell spheres per unit length along the cylinder axis. As the cylinder diameter D expands from a perfect, close packed shell, the shell could expand radially and compress axially, but it is always preferable for a line slip to emerge instead[40]. It is
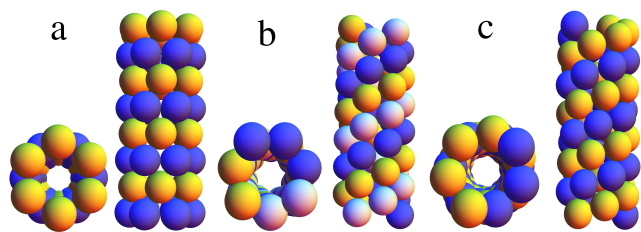
Fig. 5 Perfect, close packed outer shells: (a) stacked layers of 6 spheres each (6,6,0), (b) a 7-particle triple helix (7,4,3), and (c) a 7-particle double helix (7,5,2).
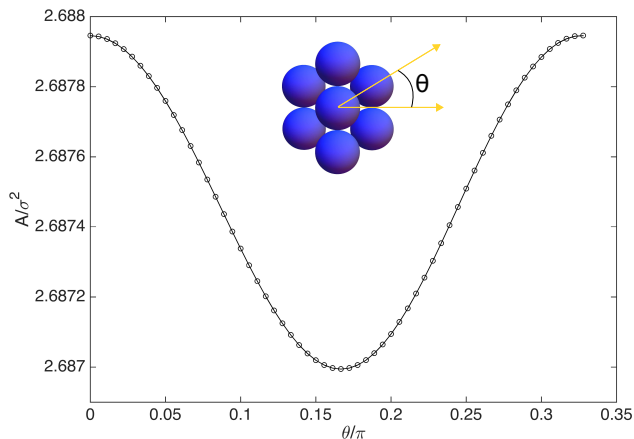
Fig. 6 The cylinder surface area occupancy for bent hexagons with different orientations for $D = 3\sigma$. The area coverage is minimized for $\theta = \pi/6$ and is maximal for $\theta = 0$, even though it is the latter structure that gives rise to the (6,6,0) outer shell.

an exercise in geometry to analytically generate these structures. The density of the inner core, ρ_∞, is then computed as follows. (i) We sample all of the possible heights for a periodic starting point within the helix periodicity, looking for a combination of r and θ that maximizes r while obeying the hard sphere and hard wall constraints. (ii) Given the position of a sphere in the core, we then assume the best way to pack the next higher sphere is to place it at the lowest possible position without moving any sphere in the shell or already placed in the core. Each core sphere thus touches the core sphere below it and two spheres of the outer shell. (iii) We iterate this step until the density of the core can be determined to within the desired numerical accuracy.

Overall, we thus assume that the core density is optimized by maximizing the radial coordinates of the inner particles, and especially the first one. This last assumption is made with no loss of generality for the cases in which the core is quasiperiodic, as in such cases every height of a core particle relative to the shell structure is approached with arbitrary accuracy in the infinite system; the value obtained for ρ_∞ does not depend on the location of the initial particle. We also assume that a locally densest packing ensures a globally densest packing. This last assumption is known not to be true in general. For random-sequential addition, for instance, it is known to fall far short of the close packing[41]. The highly constrained nature of our growth algorithm, however,

here does give access to very high density structures.

In the special case $D = 3\sigma$, the procedure can be described by a map. Recall that $\Delta_\perp = \sigma\sqrt{\sqrt{3}-1}$ is the spacing between successive layers of the shell. Consider a core sphere at a generic specified height z_1 that is moved as far as possible off of the cylinder axis and is therefore touching two shell spheres. Let $\boldsymbol{x}_1$ be the position of this sphere and $\boldsymbol{x}_2$ be the position of the core sphere that sits just above it. Let $a_i = \{z_i/\Delta_\perp\}$, where $\{\cdot\}$ denotes the fractional part, indicate the relative height of the ith sphere with respect to the shell layers just below and just above it. We construct the map $M(a)$ that relates a_2 to a_1. This map can then be iterated to determine the locations of all of the spheres in the core:

$$z_{i+1} = z_i + (1 + \{a_2 - a_1\})\Delta_\perp . \tag{16}$$

If the map converges to a fixed point or a limit cycle, the core is periodic. We will see, however, that this map is either quasiperiodic or has an extremely long period.

Figure 7 shows the possible locations $\boldsymbol{x}_1$ for a sphere within one layer. The cyan circular arc shows the possible locations for a sphere that touches two adjacent shell spheres in a same layer. The magenta arc shows the possible locations for a sphere that touches two adjacent spheres in different layers. The purple arc shows the same locations as the cyan arc, but shifted up one layer and rotated accordingly by $\pi/6$ about the cylinder axis. The portions of these arcs shown with thick blue and red curves (along with the positions related by the hexagonal rotations and reflections) are the possible locations of a core sphere within the depicted layer.
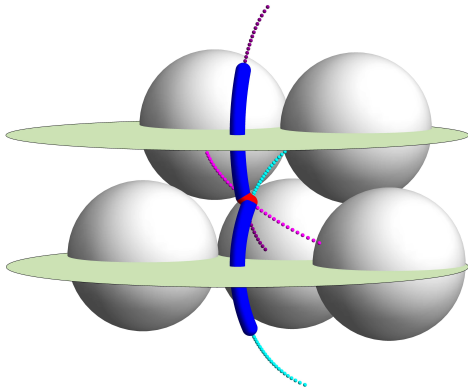
Fig. 7 Possible locations of a core sphere within a layer. The large disks are cross sections of the confining cylinder, and are separated by $\Delta_\perp$. The core sphere must be centered on a point on one of the thick blue curves or the short, thick red curve. See text for details.

The placement, $\boldsymbol{x}_2$, of the sphere that rests on top of the sphere at $\boldsymbol{x}_1$ must lie on a piecewise arc of the type shown in Fig. 7, displaced one or two layers upward, and rotated so as to be as close to diametrically opposite $\boldsymbol{x}_1$ as possible. Inspection of the possible rotations and reflections reveals that the choice leading to the densest structure is a reflection through the plane containing the cyan arc in Fig. 7, followed by a rotation by $7\pi/6$ about the

cylinder axis and a translation upward by $\Delta_\perp$, as shown in Fig. 8.
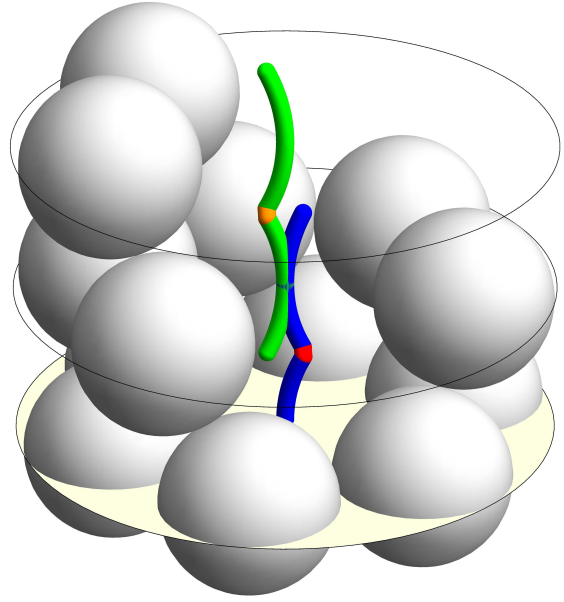
Fig. 8 Placement of a core sphere. A point P on the blue or red curve indicates a possible placement of a sphere center. The sphere above it lies on the point on the green or orange curve that is a distance σ from P. See text for details.

The map $M(a)$ is determined by finding the value of a_2 along the upper curve (green/orange in Fig. 8) that is exactly σ away from a_1 on the lower curve (blue/red). $M(a)$ has the form of a circle map:

$$M(a) = \{a + \omega + f(a)\} , \tag{17}$$

where ω is a constant and $f(a)$ is a periodic function with unit period and zero mean. Numerical computation of the map yields $\omega = 0.163887$ and the function $f(a)$ shown in Fig. 9. Note the scale on the vertical axis; deviations from a line with unit slope are quite small. The slope of $M(a)$ lies within the range $(0.8689, 1.1533)$ everywhere, hence the map is monotonic and thus invertible, which means that it cannot be chaotic[42].

For a circle map with a small amplitude nonlinearity, the generic behavior is quasiperiodic[42]. In the present case, we confirm the quasiperiodicity to a high degree of accuracy, i.e., we detect no exponential convergence to a limit cycle, and we determine the asymptotic density ρ_∞ by fitting the values of $\rho_n = n/z_n$ to the form

$$\rho_\infty = \rho_n + c/n, \tag{18}$$

where c is a fitting constant. More precisely, we compute z_n, the height of the nth sphere in the core, taking $z = 0$ to be a point at the center of a layer of the outer shell and beginning with $z_1 = 0$. We then extract the sequence of z_n values for which the nth sphere sets a new record for coming closest to lying exactly in the
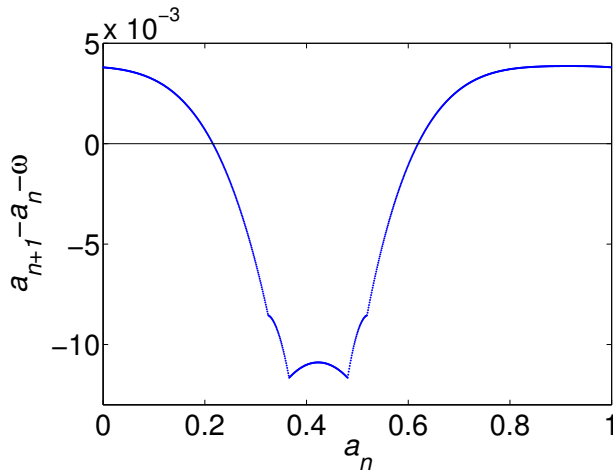
Fig. 9 Plot of the nonlinear term in the map from the height of one core sphere to the next one up, $f(a)$. Note that for the purposes of this figure we have not taken the fractional part of a_{n+1}. Note also the scale on the vertical axis.

plane of a layer, but is just below that plane, i.e, points for which a_n comes ever closer to unity. Note that if the sequence were converging to a periodic limit cycle, this procedure would either yield a finite sequence or one that exponentially approaches a value different from unity. Figure 10 shows $\rho_n - \rho_\infty$ as a function of n for the sequence of best approximants, where ρ_∞ has been adjusted to get a straight line on the log-log plot. We find the best fit to be obtained for $\rho_\infty \approx 1.0043324(1)/\sigma$, which is slightly denser than for a simple stack of spheres on the cylinder axis, $1/\sigma$. The total number of spheres per unit of cylinder length is thus $\rho_s + \rho_\infty = 8.0169578(1)/\sigma$, corresponding to $\eta = 0.593849(1)$, which is denser than $\eta = 0.593661(1)$ obtained from the SLP algorithm, as expected.
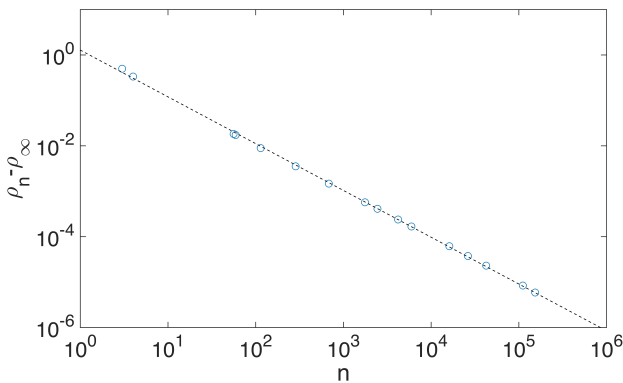
Fig. 10 Infinite-system size extrapolation of the core linear density to ρ_∞ for $D = 3\sigma$ from the sinking algorithm fitted to Eq. (18).

For $D \neq 3\sigma$, the lack of reflection symmetry in the helical shells and the presence of line slips complicate the construction of a map from one core sphere height to the next. We instead perform brute force numerical computations of the core packing algorithm for n spheres and take the core density to be $\rho_n = n/z_n$. The core density, ρ_∞, is obtained by fitting the numerical results to Eq. (18),

as above. The joint core and shell packing fraction, $\eta(D)$, is then obtained with a resolution of $\Delta D = 0.001\sigma$ (see Fig. 11).

For most values of D, the sinking algorithm gives structures with a higher packing fraction than the SLP algorithm, but differences that are typically less than 0.1%, which suggests that the SLP algorithm performs remarkably well in this regime. The most significant structural difference between the two algorithms is observed for $3.003\sigma \leq D \leq 3.017\sigma$, where the sinking algorithm identifies structures with a (7,4,3) outer shell, while the SLP algorithm produces a (6,6,0) outer shell. The packing fraction difference between these two structures is small, but well above our numerical precision. The discrepancy may thus result from the former structure not being as easily accessible in the SLP search than the latter for our choice of algorithmic parameters and initial conditions.

At the level of precision considered for the SLP study ($\Delta D = 0.01\sigma$), the sinking algorithm is found not to win outright at three points: $D = 3.04\sigma$, $D = 3.27\sigma$, and $D = 3.40\sigma$ (see Table 2). We find that two distinct mechanisms are at play, which can be seen through consideration of the linear density ratio between the SLP and the sinking algorithms separately for the shell, ρ_s, and for the core, ρ_∞ (Fig. 11 inset). Interestingly, we find that $\rho_s^{SLP}/\rho_s^{sink} \leq 1$ at 3.04σ and 3.40σ. This indicates that a denser core is obtained at the expense of having a slightly perturbed (and less dense) outer shell. At 3.27σ, some shell spheres instead do not touch the cylinder wall (taking over some of the empty core space), which increases both the shell and the core densities. (For $D = 3.09 - 3.10\sigma$, the SLP also identifies a denser outer shell than the one used in the sinking algorithm, but in these cases the denser core obtained by the sinking algorithm more than compensates for this difference.) The effect of the coupling between the outer shell and the inner core may be due to the proximity of a change to the shell symmetry ($D \approx 3.04\sigma$), or to the end of this regime ($D \approx 3.40\sigma$), but finer resolution studies would be needed to make more definitive statements. It is also unclear whether this coupling is strong enough to make the close packed structures periodic. SLP identifies unit cells that contain at least $55 \leq N \leq 80$ spheres, but larger cells are certainly possible.

Table 2 Density differences between SLP and sinking structures for points where the former is denser than the latter.

D/σ	$(\rho_s^{SLP} - \rho_s^{sink})\sigma$	$(\rho_\infty^{SLP} - \rho_\infty^{sink})\sigma$	$\eta^{SLP} - \eta^{sink}$
3.04	-6.4×10^{-6}	1.259×10^{-3}	9.0×10^{-5}
3.27	2.9×10^{-6}	4.510×10^{-4}	2.8×10^{-5}
3.40	-7.9×10^{-3}	9.254×10^{-3}	7.2×10^{-5}

5 Conclusion

In this study, we have extended the range of known HS close packings in cylinders of diameters $D = 2.862\sigma$ to $D = 4.00\sigma$ by adapting the SLP method of Ref. [34] to this geometry and by developing a sinking algorithm. We have identified 17 new structures, most of them chiral, along with their continuous deformation. We also distinguish ranges of cylinder diameters over which different types of packings are observed. Most notably, around $D = 3\sigma$ the outer shell is both fairly independent of the inner core and close
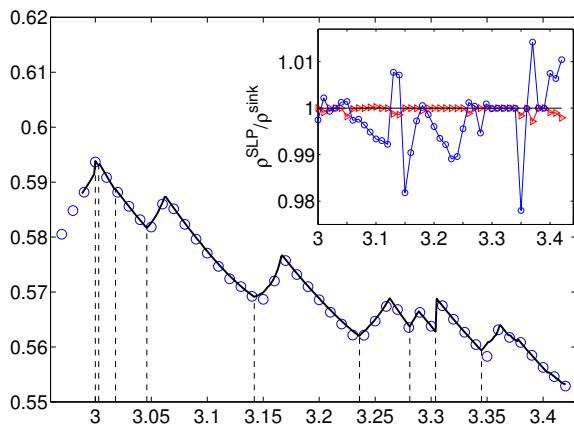
Fig. 11 Packing results for the SLP (blue circles) and the sinking (solid line) algorithms are in fairly close agreement, but the quasiperiodic phases identified by the latter are typically denser. The biggest differences are in the choice of optimal shell morphology around $D = 3.01\sigma$ and $D = 3.35\sigma$. The phase sequence for the sinking algorithm is (7,4,3), (6,6,0), (7,4,3), (6,6,0), (7,5,2), (7,6,1), (8,4,4), (8,5,3), (7,7,0) and (8,6,2), from left to right (separated by dashed lines). The inset shows the shell $\rho_s^{SLP}/\rho_s^{sink}$ (red triangles) and core $\rho_\infty^{SLP}/\rho_\infty^{sink}$ (blue circles) linear density ratio as a function of D. See text for details.

packed, and both algorithms provide strong numerical evidence that many of the packings are quasiperiodic.

Although our study ended at $D = 4.00\sigma$, we expect the competition between different shells to persist even once three and four of them develop. For $D \gg 4\sigma$, however, the bulk FCC limit should eventually be recovered. The shell area should thus eventually form but a thin wrapping of a FCC core. Based on the analogy with packing of disks within a circle[15], however, we don't expect this phenomenon to develop before $D \gtrsim 20\sigma$, which is far beyond the regime that can be reliably studied with existing numerical methods.

In closing, it is important to recall the difference between packings and their assembly from local algorithms, such as the Lubachevsky-Stillinger algorithm[43] and other slow annealing approaches that mimic self assembly. Although optimal, some of the packings may be dynamically hard to access (or even inaccessible) via self-assembly, which can be important in simulations and colloidal experiments. This question will be the object of a future publication.

Acknowledgments

References

1 M. Hifi and R. M'hallah, Adv. Oper. Res., 2009, **2009**, 150624.

2 A. B. Hopkins, Y. Jiao, F. H. Stillinger and S. Torquato, Phys. Rev. Lett., 2011, **107**, 125501.

3 L. Filion and M. Dijkstra, Phys. Rev. E, 2009, **79**, 046714.

4 J. K. Kummerfeld, T. S. Hudson and P. Harrowell, J. Phys. Chem. B, 2008, **112**, 10773–10776.

5 K. Zhang, W. W. Smith, M. Wang, Y. Liu, J. Schroers, M. D. Shattuck and C. S. O'Hern, Phys. Rev. E, 2014, **90**, 032311.

6 T. Aste and D. Weaire, The Pursuit of Perfect Packing, Taylor and Francis, New York, 2nd edn, 2008.

7 T. C. Hales, Ann. Math., 2005, 1065–1185.

8 J. H. Conway and N. J. A. Sloane, Sphere Packings, Lattices and Groups, Springer-Verlag, New York, 3rd edn, 1999, vol. 290, p. 663.

9 H. Cohn and N. Elkies, Ann. Math., 2003, **157**, 689.

10 Y. G. Stoyan, Advances in CAD/CAM: Proceedings of PROLAMAT82, Leningrad, USSR, 1982, 67–86.

11 H. J. Fraser and J. A. George, Eur. J. Oper. Res., 1994, **77**, 466–474.

12 L. H. W. Yeung and W. K. Tang, IEEE Trans. Ind. Electron., 2005, **52**, 617–627.

13 R. L. Graham, B. D. Lubachevsky, K. J. Nurmela and P. R. Östergaard, Discrete Math., 1998, **181**, 139–154.

14 F. Fodor, Beitrage Algebra Geom., 2003, **44**, 431–440.

15 A. B. Hopkins, F. H. Stillinger and S. Torquato, Phys. Rev. E, 2010, **81**, 041305.

16 H. Akeb and M. Hifi, Comput. Oper. Res., 2013, **40**, 1243–1255.

17 Y. G. Stoyan and G. Yas' kov, Eur. J. Oper. Res., 2004, **156**, 590–600.

18 M. Goldberg, Math. Mag., 1971, 199–208.

19 T. Gensane, Electron. J. Combin., 2004, **11**, R33.

20 Y. Y. Stoyan, G. Yaskow and G. Scheithauer, Central Eur. J. Oper. Res., 2003, **11**, 389–407.

21 P. Pieranski, L. Strzelecki and B. Pansu, Phys. Rev. Lett., 1983, **50**, 900–903.

22 M. Schmidt and H. Löwen, Phys. Rev. Lett., 1996, **76**, 4552–4555.

23 A. Fortini and M. Dijkstra, J. Phys.: Condens. Matter, 2006, **18**, L371.

24 W. Mickelson, S. Aloni, W.-Q. Han, J. Cumings and A. Zettl, Science, 2003, **300**, 467–469.

25 A. N. Khlobystov, D. A. Britz, A. Ardavan and G. A. D. Briggs, Phys. Rev. Lett., 2004, **92**, 245507.

26 M. Tymczenko, L. F. Marsal, T. Trifonov, I. Rodriguez, F. Ramiro-Manzano, J. Pallares, A. Rodriguez, R. Alcubilla and F. Meseguer, Adv. Mater., 2008, **20**, 2315–2318.

27 S. Sanwaria, A. Horechyy, D. Wolf, C.-Y. Chu, H.-L. Chen, P. Formanek, M. Stamm, R. Srivastava and B. Nandan, Angew. Chem. Int. Ed., 2014, **53**, 9090–9093.

28 R. Liang, J. Xu, R. Deng, K. Wang, S. Liu, J. Li and J. Zhu, ACS Macro Lett., 2014, **3**, 486–490.

29 K. S. Troche, V. R. Coluci, S. F. Braga, D. D. Chinellato, F. Sato, S. B. Legoas, R. Rurali and D. S. Galvão, Nano Lett., 2005, **5**,

349–355.

30 V. N. Bogomolov, Y. A. Kumzerov, V. P. Petranovskii and A. V. Fokin, Sov. Phys. Crystallogr., 1990, **35**, 197–198.

31 G. T. Pickett, M. Gross and H. Okuyama, Phys. Rev. Lett., 2000, **85**, 3652.

32 A. Mughal, H. Chan, D. Weaire and S. Hutzler, Phys. Rev. E, 2012, **85**, 051305.

33 H.-K. Chan, Phys. Rev. E, 2011, **84**, 050302.

34 S. Torquato and Y. Jiao, Phys. Rev. E, 2010, **82**, 061302.

35 A. Makhorin, GLPK (GNU linear programming kit), 2008.

36 H. C. Huang, S. K. Kwak and J. K. Singh, J. Chem. Phys., 2009, **130**, 164511.

37 A. Mughal, H. K. Chan and D. Weaire, Phys. Rev. Lett., 2011, **106**, 115704.

38 U. Pirl, Math. Nachr., 1969, **40**, 111–124.

39 H. Melissen, Geod. Dedic., 1994, **50**, 15–25.

40 A. Mughal and D. Weaire, Phys. Rev. E, 2014, **89**, 042307.

41 S. Torquato, Random heterogeneous materials: microstructure and macroscopic properties, Springer Science & Business Media, 2013, vol. 16.

42 E. Ott, Chaos in dynamical systems, Cambridge University Press, Cambridge, New York, 2002.

43 B. D. Lubachevsky and F. H. Stillinger, J. Stat. Phys., 1990, **60**, 561–583.

Table of Content Entry

a   b   c
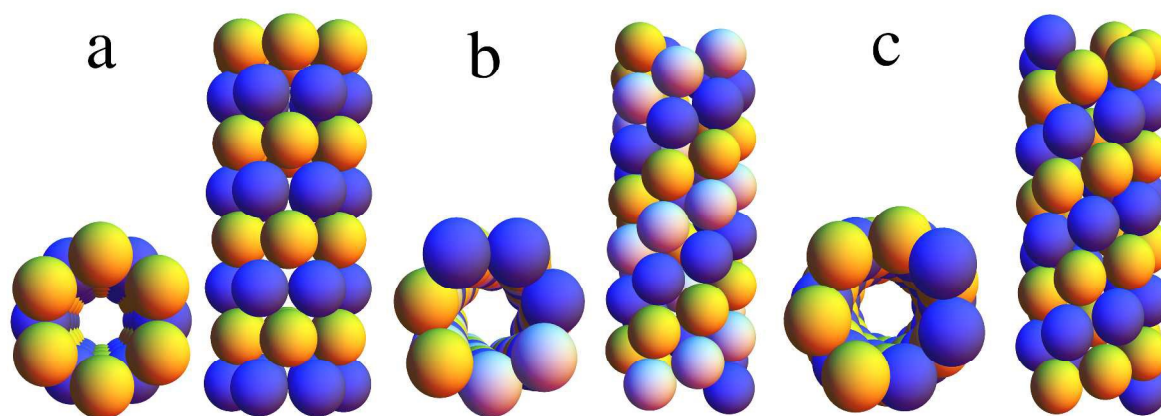
We extend the identification of close packings up to D = 4.00σ and find 17 new structures.